Catalysis Today 192 (2012) 67–71

Contents lists available at SciVerse ScienceDirect

Catalysis Today

journal homepage: www.elsevier.com/locate/cattod

Highly active and selective supported bulk nanostructured MoVNbTeO catalysts for the propane ammoxidation process

R. López-Medina [a], E. Rojas [a], M.A. Bañares [a], M.O. Guerrero-Pérez [b,*]

[a] Catalytic Spectroscopy Laboratory, Instituto de Catálisis y Petroleoquímica, CSIC, Marie Curie 2, E-29049 Madrid, Spain
[b] Departamento de Ingeniería Química, Universidad de Málaga, E-29071 Málaga, Spain

ARTICLE INFO

Article history:
Received 1 August 2011
Received in revised form 24 October 2011
Accepted 9 November 2011
Available online 15 December 2011

Keywords:
Propane
Acrylonitrile
Nanostructured-catalysts
MoVNbTeO
Supported bulk oxides
M1

ABSTRACT

We report a methodology to prepare nanoscaled supported-bulk MoVNbTeO catalysts in which the phases required to obtain an active and selective catalysts are nanoscaled on the surface of a support. Thus, a more economic catalytic material with improved mechanical properties can be obtained. The effect of vanadium content and atmosphere of calcination on the catalytic performance are discussed, and the results of the supported-catalysts are compared with those of bulk catalytic samples, which have been prepared as reference. The best supported catalyst afford ca. 50% acrylonitrile yield with 80% propane conversion at 450 °C. The activity per gram of MoVNbTeO increases fourfold upon stabilization of its nanoparticles.

1. Introduction

Nanostructured catalysts present valuable advantages for both industrial and academic points of view [1], and nanoscaled particles trigger the surface to volume ratio, leading to a higher number of exposed sites for a given amount of catalyst (Scheme 1), however, this would be a short-term benefit since these may sinter into larger particles, and loose nanoparticles present additional problems. Loose nanoparticles impose constrains on security, health and handling. A good option is to immobilize nanoparticles on larger support particles (Scheme 1); thus, the active phases can be stabilized versus synterization on less-expensive materials that act as support [2]. This brings a multiple benefits since it minimizes health risk upon immobilization of nanoparticles, facilitates its handling, improves the catalyst bed mechanical properties and most relevant to catalysis, minimizes the synterization of nanoparticles into larger ones during reaction conditions [3]. The amount of active phase required for a satisfactory catalytic performance, can be significantly decreased, and, in addition, the use of nano-scaled oxide phases maximizes the surface-to-volume ratio allowing a better insight on the nature of the active phase [4–8].

Acrylonitrile is currently the second largest product from propylene, after polypropylene [9,10], with principal applications in the production of acrylic fibres, ABS (acrylonitrile–butadiene–styrene) resins, and SAN (styrene–acrylonitrile) resins, include acrylamide, adiponitrile, and nitrile elastomers. Currently, it is commercially obtained from propylene through the SOHIO process, which involves the conversion of propylene, ammonia and oxygen into acrylonitrile in a fluid bed. Nowadays there is major interest in developing the direct ammoxidation of propane into acrylonitrile, since the paraffin can be easy obtained from natural gas and is much more abundant and less expensive than the olefin. Mo–V–Te–(Nb)–O multioxide mixed metal catalysts have been described as selective for the ammoxidation of propane to acrylonitrile by several authors [11–21]. Although there is much work done regarding this catalytic system, the major effort has been done in preparing bulk catalytic materials. Our approach is to develop supported nanoscaled bulk multioxide catalysts, which performs at least like its bulk counterpart. This would also result in a system where it is possible to assess the relevance of non-crystalline surface oxide species.

2. Experimental

MoVTeNbOx mixed oxides have been prepared starting from slurries obtained by mixing aqueous solutions of the metal components. The catalysts named as $Mo_5V_4Nb_{0.5}Te_{0.5}O$-N (nitrogen) and $Mo_6V_3Nb_{0.5}Te_{0.5}O$-A (air) with a final Mo/V/Te/Nb atomic ratio of 0.5–0.6/0.4–0.3/0.05/0.05 were prepared from aqueous slurries of the corresponding salts, as reported elsewhere [22], and calcined at

* Corresponding author.
E-mail address: oguerrero@uma.es (M.O. Guerrero-Pérez).

0920-5861/$ – see front matter © 2011 Elsevier B.V. All rights reserved.
doi:10.1016/j.cattod.2011.11.018

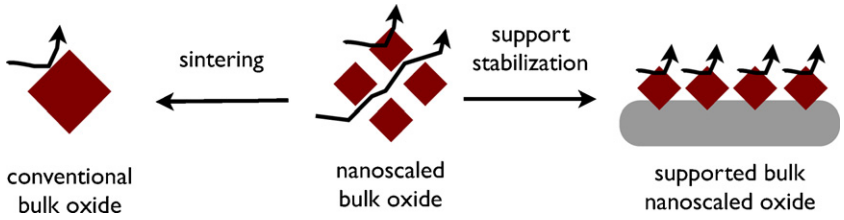

Scheme 1. Bulk catalyst nanoparticles are illustrated in the middle. Leftwards arrow illustrates sintering phenomena occurring during reaction. Rightwards arrow illustrates support-stabilized bulk nanoparticles.

Table 1
The surface properties of the MoVNbTeO catalysts measurement by XPS and N_2 fisisorption (S_{BET}). The number in brackets indicates the percentage of the peak as calculated during deconvolution.

Catalysts	Mo^{6+} $3d_{5/2}$	Mo^{5+} $3d_{5/2}$	Mo^{4+} $3d_{5/2}$	V^{5+} $2p_{3/2}$	V^{4+} $2p_{3/2}$	Te^{6+} $3d_{5/2}$	Te^{4+} $3d_{5/2}$	Nb^{5+} $3d_{5/2}$	S_{BET} (m^2/g)
$Mo_5V_4Nb_{0.5}Te_{0.5}O$-N	233.0 (50.9)	231.6 (39.1)	229.5 (10)	517.1 (70.4)	516.7 (29.6)	576.9 (86.4)	574.3 (13.6)	207.0	123
$Mo_5V_4Nb_{0.5}Te_{0.5}O$-A	232.6 (94.0)	231.7 (6.0)	–	517.5	–	577.0 (93.7)	574.2 (6.3)	207.1	74
$Mo_6V_3Nb_{0.5}Te_{0.5}O$-N	232.9 (52.0)	231.6 (42.0)	229.6 (6.0)	517.3 (91.5)	516.6 (8.5)	576.6 (87.3)	574.2 (12.7)	206.8	125
$Mo_6V_3Nb_{0.5}Te_{0.5}O$-A	232.7 (96.0)	231.7 (4.0)	–	517.3 (81.4)	516.6 (18.6)	576.9 (94.0)	574.3 (6.0)	206.9	82

600 °C for 2 h in N_2 and air flow. They were prepared in order to have a total Mo + V + Nb + Te coverage of 12 atoms per nm^2 on alumina support, which is roughly two monolayers coverage. As references, two bulk samples were prepared following the same procedure but without adding alumina support, named as $Mo_5V_4Nb_{0.5}Te_{0.5}O$-N-bulk and $Mo_6V_3Nb_{0.5}Te_{0.5}O$-N-bulk.

Powder X-ray diffraction analyses were carried out using a X'Pert Pro PANalytical Siemens D500 diffractometer employing Cu Kα radiation (λ = 0.15418 nm) and a graphite monochromator. BET specific surface areas were measured on a Micromeritics ASAP-2000 apparatus. Prior to the adsorption experiments, samples were outgassed at 140 °C for 2 h. X-ray photoelectron spectroscopy (XPS) experiments were carried out on a VG Escalab 200R spectrometer using Mg Kα radiation (Mg Kα = 1254.6 eV) X-ray source, powered at 120 W. Raman spectra were collected in a Renishaw System 1000 spectrometer equipped with Ar ion laser (Spectra Physics, λ = 514 nm, power 19 mW, 1 mW on sample) and a cooled CCD detector (−73 °C). The spectral resolution was ca. 3 cm^{-1} and spectrum acquisition consisted of 10 accumulations of 30 s. The spectra were obtained under dehydrated conditions (200 °C) in a hot stage (Linkam TS-1500) in synthetic dry air flow.

The catalytic experiments were carried out in a fixed-bed quartz tubular reactor with feed composition (vol.%) $C_3H_8/O_2/NH_3$/He of 9.8/25/8.6/56.6, 0.2 g of catalyst with particle dimensions 0.25–0.125 mm, and total flow rate of 20 ml/min; in the 350–500 °C temperature range, at atmospheric pressure, with an on-line GC Varian CP-3800 These reaction conditions were selected in order to avoid internal and external diffusion limitations. The axial reaction temperature profile was monitored by a thermocouple inserted into the catalytic bed. The accuracy of the analytical determinations was checked for each test by verification that the carbon balance was within the accumulative mean error of the determination.

3. Results

The BET area values (Table 1) are quite low in the catalysts calcined in air compared to the values obtained for the samples treated under inert atmosphere. This fact has been found before with similar catalysts and was observed for different catalysts composition [22,23]. Since in this case the coverage is up to twice monolayer coverage (ca. 12 atoms/nm^2), this could be indicative that a layer of porous oxide structure develops over the alumina support in the case of the inert atmosphere treatment.

XPS results are presented in Table 1. The procedure for the peak fitting and assignation of the binding energy values to the different oxidation states have been described previously [22]. The Mo $3d_{5/2}$ binding energy (BE) values suggest that Mo^{6+}, Mo^{5+} and Mo^{4+} are present in the catalysts calcined in nitrogen flow, although the percentage of Mo^{4+} is quite low. However, only Mo^{6+} and Mo^{5+} are present in the samples calcined in air flow, and the amount of Mo^{5+} species is very low. The BE values for V $2p_{3/2}$ peak are around 517.5–516.6 eV, that can be fitted into two components at 517.1–517.5 eV and ~516.6 eV, respectively, which can be related to V^{5+} and V^{4+} species, respectively. The data indicate that the major part of vanadium species are in their highest oxidation state, although some species remain reduced as V^{4+}. The Te $3d_{5/2}$ peak at 576.6–577.0 eV corresponds to Te^{6+} in all the cases.

Figs. 1 and 2 show the XRD patterns of fresh and used catalysts. In the case of inert-calcined fresh samples (Fig. 1) MoO_2 and a rutile Mo–V–Nb–Te–O phase [24] are detected, along with the pattern of mixed phases containing Te, M1, M2 and $Te_2M_{20}O_{57}$. In should be noted that the pattern of MoO_2 oxide is not visible after use in propane ammoxidation reaction. The presence of this oxide in the inert calcined samples (which possesses Mo^{4+}) is in agreement with XPS (Table 1). For the air-calcined samples (Fig. 2), several peaks in the 22–30° range correspond to mixed Al–Mo–O, Mo–Nb–O and Mo–V–O phases. It should be noted that mixed phases containing alumina are only detected for air-calcined samples, which also exhibit tellurium-containing phases. No peaks corresponding to

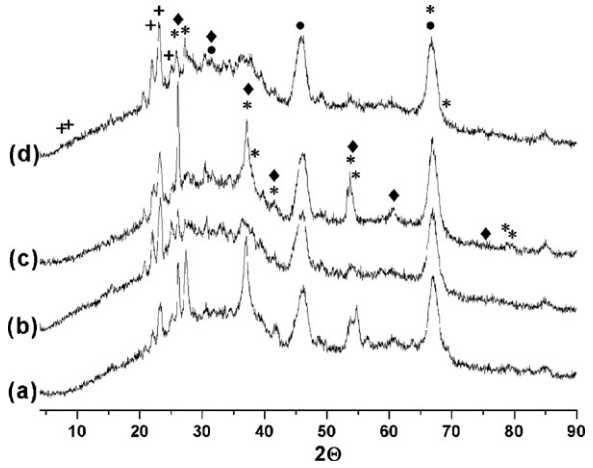

Fig. 1. XRD patterns of fresh and used catalysts; (a) $Mo_5V_4Nb_{0.5}Te_{0.5}O$-N fresh, (b) $Mo_5V_4Nb_{0.5}Te_{0.5}O$-N used, (c) $Mo_6V_3Nb_{0.5}Te_{0.5}O$-N fresh and (d) $Mo_6V_3Nb_{0.5}Te_{0.5}O$-N used. (*) MoVNbO rutile, (+) $Te_2M_{20}O_{57}$ M1-phase, (♦) MoO_2, (•) γ-Al_2O_3.

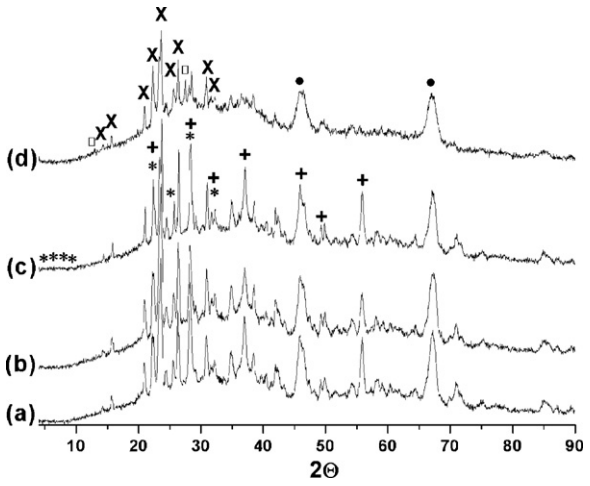

Fig. 2. XRD patterns of fresh and used catalysts; (a) $Mo_5V_4Nb_{0.5}Te_{0.5}O$-A fresh, (b) $Mo_5V_4Nb_{0.5}Te_{0.5}O$-A used, (c) $Mo_6V_3Nb_{0.5}Te_{0.5}O$-A fresh and (d) $Mo_6V_3Nb_{0.5}Te_{0.5}O$-A used. (X) $Al_2(MoO_4)_3$, (*) $Te_2M_{20}O_{57}$ M1-phase, (+) $Te_{0.33}MO_{3.33}$ M2-phase, (□) α-MoO_3, (•) γ-Al_2O_3.

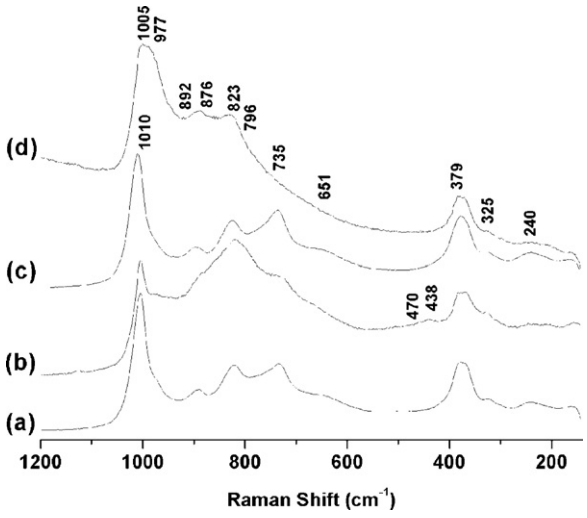

Fig. 4. *In situ* dehydrated Raman spectra (200 °C) of (a) $Mo_5V_4Nb_{0.5}Te_{0.5}O$-A fresh and (b) used, (c) $Mo_6V_3Nb_{0.5}Te_{0.5}O$-A fresh and (d) used in the amoxidation of propane to obtain acrylonitrile.

V_2O_5, MoO_3 or Nb_2O_5 are detected in the patterns of fresh samples and only a weak peak that can be assigned to the pattern of MoO_3 oxide is visible in used $Mo_6V_3Nb_{0.5}Te_{0.5}O$-A catalyst.

Figs. 3 and 4 show the Raman spectra of fresh and used dehydrated samples. All of them present a strong signal near 990–1030 cm^{-1}, characteristic of the stretching modes of Mo=O and/or V=O bonds, respectively (25). The Mo=O signal appears near 990 whereas the band corresponding to V=O bonds appears near 1020 cm^{-1}. In any case, it is difficult to assess the relative population of Mo=O and V=O sites since the Raman section of molybdenum oxide species is more intense than that of vanadium oxide [25]. For inert treated samples (Fig. 3), the signal near 990 cm^{-1} in the fresh sample shifts to higher energies after reaction, which could indicate a higher population of molecularly dispersed Mo or V oxides. This is not observed in the case of air calcined samples (Fig. 4). The band near 380 cm^{-1}, visible in all the samples, belongs to a Mo–V–O phase [22,23]. Both catalysts calcined in nitrogen exhibits Raman bands near 820 and 470 cm^{-1}, which are characteristic of M1 phase [21]. M2 phase exhibits a band near 440 cm^{-1} [26], which is hardly visible in some samples. The broad signal near 820 cm^{-1}, visible in all the samples, corresponds to the rutile-type structure, whereas the signal near 880–890 cm^{-1} can be assigned to the stretching mode of bridging Mo–O–M (M = Mo, V) bonds of highly distorted $Te_2M_{20}O_{57}$ on alumina [27–29].

Fig. 5 shows propane conversion and the yield to acrylonitrile obtained on supported catalysts as a function of the reaction temperature. Acetonitrile, propylene, CO and CO_2, with traces of acrolein, acetone and acetic acid, were also detected. As a general trend, when the reaction temperature increases, the conversion of propane and selectivity to acrylonitrile increase, reaching a maximum near 450 °C. The yields to acrylonitrile obtained are higher in the case of inert calcined samples. In both cases, higher vanadium content ($Mo_5V_4Nb_{0.5}Te_{0.5}O$-A and $Mo_5V_4Nb_{0.5}Te_{0.5}O$-N) results in higher propane conversion and acrylonitrile yield values. Fig. 6 illustrates the activity results obtained for propane ammoxidation on the inert calcined supported samples and for the two bulk samples that have been prepared as reference. The rutile structure was detected in the bulk samples by both Raman spectroscopy and XRD (additional support information). It can be clearly observed how the

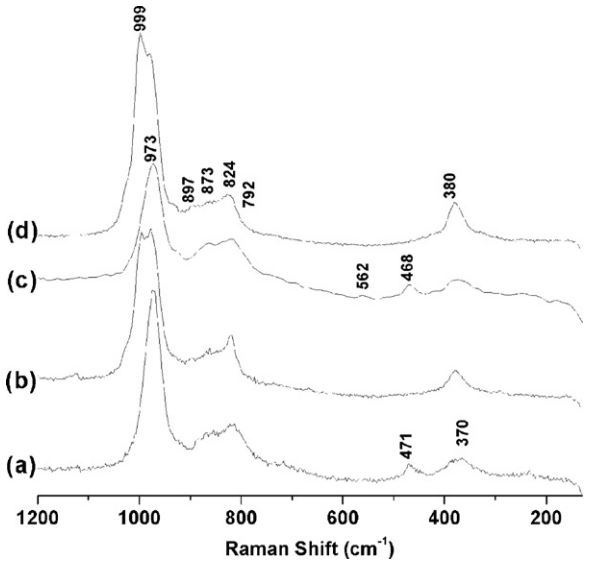

Fig. 3. *In situ* dehydrated Raman spectra (200 °C) of (a) $Mo_5V_4Nb_{0.5}Te_{0.5}O$-N fresh and (b) used, (c) $Mo_6V_3Nb_{0.5}Te_{0.5}O$-N fresh and (d) used in the amoxidation of propane to obtain acrylonitrile.

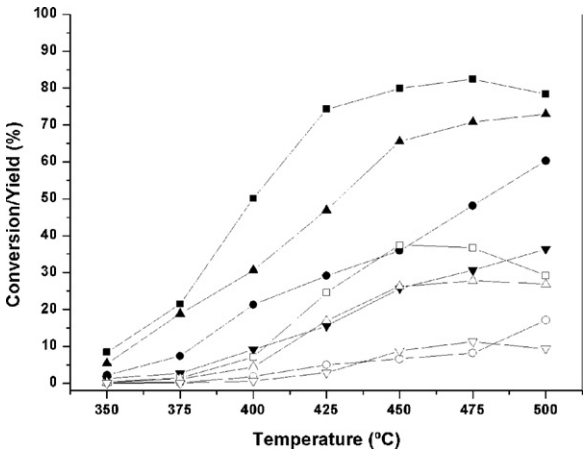

Fig. 5. . Catalytic performance of conversion in the amoxidation of propane (full symbols) and yield to acrylonitrile (open symbols): (■, □) $Mo_5V_4Nb_{0.5}Te_{0.5}O$-N, (•, ○) $Mo_5V_4Nb_{0.5}Te_{0.5}O$-A, (▲, △) $Mo_6V_3Nb_{0.5}Te_{0.5}O$-N and (▼, ▽) $Mo_6V_3Nb_{0.5}Te_{0.5}O$-A.

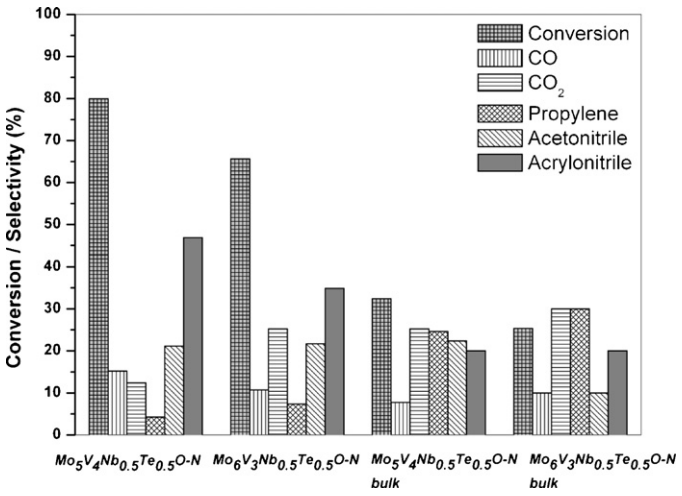

Fig. 6. Catalytic performance of conversion in the amoxidation of propane. Reaction conditions: feed composition (vol.%) $C_3H_8/O_2/NH_3/He$ 9.8/25/8.6/56.6, 0.2 g of catalyst with particle dimensions 0.25–0.125 mm, and total flow rate of 20 ml/min. $T = 450\,^{\circ}C$.

performance of the supported samples outperforms that of the bulk ones in propane conversion and in selectivity to acrylonitrile.

4. Discussion

The atmosphere calcination determines the phases present on the alumina-supported Mo–V–Nb–Te–O catalysts. The inert calcination gives rise to the presence of reduced molybdenum species, as evidenced the XPS results (Table 1), which are present mainly in the form of MoO_2, which can be also into the rutile lattice. This series exhibits higher BET surface area values (Table 1), which could be indicative that a layer of mesoporous oxide is deposited on the surface of the alumina support. Previous characterization results with methanol oxidation showed that these supported catalysts calcined in inert atmosphere present both redox and acid surface sites [23], such combination of sites is related to the good performance that these nanoscaled catalysts have shown (Fig. 6). Air-calcined series present lower surface area and tend to incorporate aluminum from the support in their structures.

The catalytic results (Figs. 5 and 6) show better performance for the catalysts with higher vanadium content. This is in agreement with previous studies about propane ammoxidation, which identifies molecularly dispersed vanadium oxide as the critical site for hydrocarbon transformation into propylene, which is the first step [30–33]. Actually, adsorbed alkoxy species have been identified during propane ammoxidation conditions, suggesting the involvement of these surface vanadium sites in the propane adsorption. Better performing catalysts exhibit stronger Raman band of vanadium alkoxide species during reaction. Recent investigations by density functional theory calculations regarding the adsorption of C3 molecules on the surface planes of M1 phase also may indicate that vanadium sites are responsible for the initial propane activation step [34].

The catalytic results reported for $Mo_5V_4Nb_{0.5}Te_{0.5}O$-N, with almost 50% of acrylonitrile yield at 80% propane conversions, are very promising, since they are in the same range than those reported with bulk MoVNbTeO mesoporous oxides [18]. The performance of the M1 pure phase has been also described in the literature, for propane conversions of 20% the selectivity to acrylonitrile is close to 35%, although the selectivity is improved when a mixture of M1 + M2 phases was used [34,35]. This underlines that not a single phase but a site associated with the coexistence of two phases is

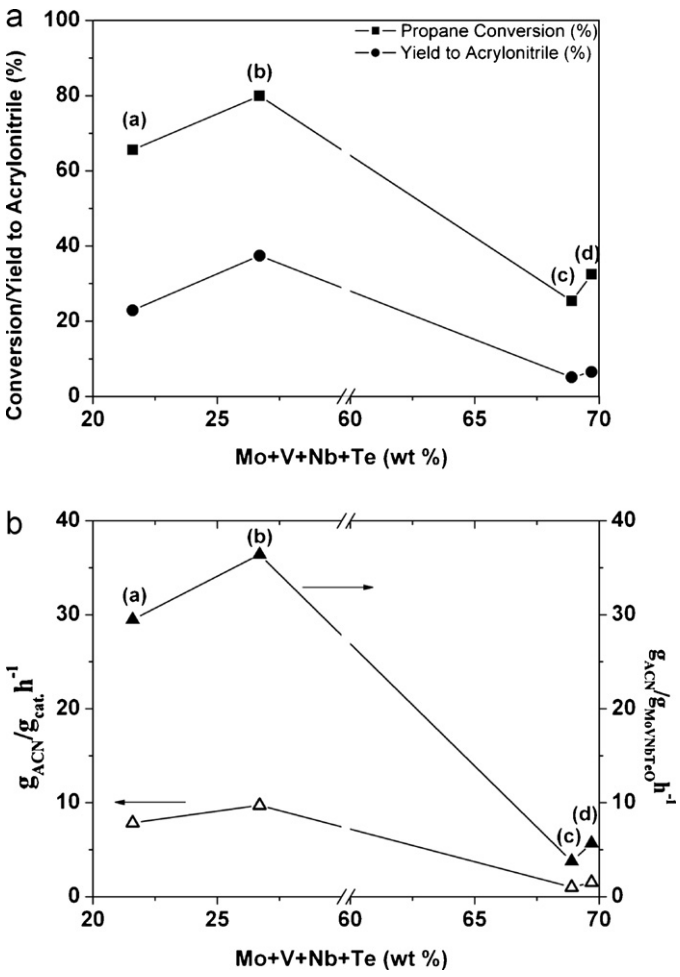

Fig. 7. (A) Propane conversion and yield to acrylonitrile versus Mo + V + Nb + Te content. (a) $Mo_6V_3Nb_{0.5}Te_{0.5}O$-N, (b) $Mo_5V_4Nb_{0.5}Te_{0.5}O$-N, (c) $Mo_6V_3Nb_{0.5}Te_{0.5}O$-N-bulk and (d) $Mo_5V_4Nb_{0.5}Te_{0.5}O$-N-bulk and (B) formation of acrylonitrile per unit mass of catalyst per unit time. Reaction conditions: feed composition (vol.%) $C_3H_8/O_2/NH_3/He$ 9.8/25/8.6/56.6, 0.2 g of catalyst with particle dimensions 0.25–0.125 mm, and total flow rate of 20 ml/min. $T = 450\,^{\circ}C$.

to be invoked as directly related to the active site. Probably, defective phases formed at the boundaries between M1 and M2 domains.

The main by-product is acetonitrile, in a similar fashion to its production during propylene ammoxidation. This fact is quite important since nowadays there has been a world shortage of this product [36], and it may be a recurrent scenario. Acetonitrile, independently from acrylonitrile, is also an important chemical intermediate that finds many applications. The supported bulk nanoscaled catalyst, with a much lower amount of MoVNbTe multioxide phase, performs better than the corresponding unsupported bulk (i.e., conventional bulk) catalysts, which have a higher amount of active oxide phase, as Fig. 7A and B illustrate. These show the formation of acrylonitrile per unit of mass of active phase (Mo + V + Te + Nb) and also per unit of time. In both cases, and for all the catalysts formulations studied, the acrylonitrile produced per gram of active phase is much higher in the case of the supported bulk nanoscaled catalysts. Thus, when the active oxide phases are nanoscaled the performance of such phases is enhanced. Supporting nanoscaled bulk catalysts improves their cost and mechanical properties; in addition, they increase the exposure of active site, triggering the activity per gram of active component. This work confirms the relevance of high exposure of sites in nanoscaled catalysts as well as the relevance of non-crystalline domains. The fact that the performance per gram of active phase is higher for the

supported nanoscaled mixed oxide catalysts underlines that optimizing its preparation may result in significantly better activity values.

5. Conclusions

A high surface area supported bulk nanoscaled multioxide catalyst can be prepared with a simple synthesis method described in this paper. The surface of the supported-catalyst presents reduced Mo sites and also of Te-containing phases that give rise to an adequate balance between acid and redox sites. Such nanoscaled phases stabilized on the surface of the support are active and selective for propane ammoxidation. This material is mechanically resistant and present better catalytic performances than their bulk counterpart, thus, a significantly lower amount of active phase is required for producing the same amount of acrylonitrile. The higher activity is due, at least, to the higher exposure of the catalyst sites to the reactions.

Acknowledgements

The Ministry of Science and Innovation (Spain) funded this study under project CTQ2008-04261/PPQ. E. Rojas and R. López-Medina thank CONACYT (Mexico) and AECID-MAE (Spain), respectively, for their Ph.D. program fellowships. The authors express their thanks to Olaf Torno (Sasol Germany GmbH) for providing alumina support. Thanks are extended to the organizers of the Group Five Symposium and guest editors of this special issue, Profs. Guido Busca and Fabrizio Cavani.

References

[1] M.O. Guerrero-Pérez, J.L.G. Fierro, M.A. Bañares, Top. Catal. 41 (2006) 43.
[2] M.O. Guerrero-Pérez, J.L.G. Fierro, M.A. Vicente, M.A. Bañares, J. Catal. 206 (2002) 339–348.
[3] M.A. Bañares, Adv. Mater., in press.
[4] M.O. Guerrero-Pérez, M.A. Bañares, J. Phys. Chem. C 111 (2007) 1315–1322.
[5] R. López-Medina, J.L.G. Fierro, M.O. Guerrero-Pérez, M.A. Bañares, Appl. Catal. A 406 (2011) 34–42.
[6] M.O. Guerrero-Pérez, M.A. Bañares, Chem. Commun. 12 (2002) 1292–1293.
[7] E. Mikolajska, E. Rojas Garcia, R. López Medina, A.E. Lewandowska, J.L.G. Fierro, M.A. Bañares, Appl. Catal. A 404 (2011) 93–102.
[8] M.O. Guerrero-Pérez, J.M. Rosas, R. López-Medina, M.A. Bañares, J. Rodríguez-Mirasol, T. Cordero, Catal Commun. 12 (2011) 989–992.
[9] R.K. Grasselli, C.G. Lugmair, A.G. Volpe Jr., Top. Catal. 50 (2008) 66.
[10] R.K. Grasselli, C.G. Lugmair, A.G. Volpe Jr., Top. Catal. 54 (2011) 595.
[11] Y.C. Kim, W. Ueda, Y. Moro-oka, Catal. Today 13 (1992) 673.
[12] D.D. Sureh, D.A. Ornoff, J.F Brazdil, L.C. Glaeser, M.S. Friendich, US Patent 47060159 (1988).
[13] C. Glaeser, J.F. Brzdil, M.A. Toft, US Patents 4843655, 4835125, 4837192 (1988).
[14] J.S. Kim, S.I. Woo, Appl. Catal. 110 (1994) 207.
[15] T. Ushikubo, K. Oshima, A. Kayou, M. Vaarkamp, M. Hatano, J. Catal. 169 (1997) 394.
[16] R.K. Grasselli, F. Trifiro, Top. Catal. 54 (2011) 587.
[17] R.K. Grasselli, W.A. Goddard, Top. Catal. 50 (2008) 1.
[18] L. Yuan, V.V. Guliants, J. Porous Mater. 16 (2009) 613–622.
[19] M.A. Carreon, V.V. Gualiants, M.O. Guerrero-Perez, M.A. Bañares, Catal. Commun. (4) (2009) 416–420.
[20] K. Muthukumar, J. Yu, Y. Xu, V.V. Guliants, Top. Catal. 54 (2011) 605–613.
[21] X. Li, D.J. Buttrey, D.A. Blom, T. Vogt, Top. Catal. 54 (2011) 614–626.
[22] R. López-Medina, J.L.G. Fierro, M.O. Guerrero-Pérez, M.A. Bañares, Appl. Catal. A 375 (2010) 55–62.
[23] R. López-Medina, H. Golinska, M. Ziolek, M.O. Guerrero-Pérez, M.A. Bañares, Catal. Today 158 (2010) 139–145.
[24] N. Haddad, E. Bordes Richard, A. Barama, Catal. Today 142 (2009) 215–219.
[25] M.A. Bañares, I.E. Wachs, J. Raman Spectrosc. 33 (2002) 359–380.
[26] B. Solsona, M.I. Vázquez, F. Ivars, A. Dejoz, P. Concepción, J.M. López-Nieto, J. Catal. 252 (2007) 271–280.
[27] X. Yang, W. Zhang, R. Feng, W. Ji, C.T. Au, Catal. Lett. 124 (2008) 288.
[28] X.J. Yang, R.M. Feng, W.J. Ji, C.T. Au, J. Catal. 253 (2008) 57.
[29] P. Botella, E. García-González, J.M. López Nieto, J.M. González-Calbet, Solid State Sci. 7 (2005) 507.
[30] R. Catani, G. Centi, F. Trifiro, R.K. Grasselli, Ind. Eng. Chem. Res. 31 (1992) 107.
[31] S. Albonetti, G. Blanchard, P. Buratin, T.J. Cassidy, S. Masetti, F. Trifirò, Catal. Lett. 45 (1997) 119.
[32] H.W. Zanthoff, S. Buchholz, Catal. Lett. 49 (1997) 213.
[33] M.O. Guerrero-Pérez, M.A. Peña, J.L.G. Fierro, M.A. Bañares, Ind. Eng. Chem. Res. 45 (2006) 4537–4543.
[34] A. Govindasamy, K. Muthukumar, J. Yu, Y. Xu, V.V. Guliants, J. Phys. Chem. C 114 (2010) 4544–4549.
[35] M. Baca, M. Aouine, J.L. Dubois, J.M.M. Millet, J. Catal. 233 (2005) 234–241.
[36] E. Rojas, M.O. Guerrero-Pérez, M.A. Bañares, Catal. Commun. 10 (2009) 1555–1557.